

# Optical Engineering

[SPIDigitalLibrary.org/oe](http://SPIDigitalLibrary.org/oe)

## **High-temperature digital image correlation method for full-field deformation measurement captured with filters at 2600°C using spraying to form speckle patterns**

Xiang Guo  
Jin Liang  
Zhengzong Tang  
Binggang Cao  
Miao Yu

# High-temperature digital image correlation method for full-field deformation measurement captured with filters at 2600°C using spraying to form speckle patterns

Xiang Guo,\* Jin Liang, Zhengzong Tang, Binggang Cao, and Miao Yu

Xi'an Jiaotong University, School of Mechanical Engineering, No. 28 Xianning Road, Xi'an, Shaanxi Province 710049, China

Xi'an Jiaotong University, State Key Laboratory for Manufacturing Systems Engineering, No. 28 Xianning Road, Xi'an, Shaanxi Province, China

**Abstract.** A method is presented for obtaining good images of a sprayed speckle pattern on specimen surfaces at high temperatures, suitable for strain measurement, by digital image correlation (DIC) using plasma spray for speckle preparation in which a bandpass filter, neutral density filters, and a linear polarizing filter are used to reduce intensity and noise in images. This is accomplished by speckle preparation through the use of plasma spray and suppression of black-body radiation through the use of filters. By using plasma spray for speckle preparation and the filters for image acquisition, the method was demonstrated to be capable of providing accurate DIC measurements up to 2600°C. The full-field stretching deformation of the specimen was determined using the DIC technique. Experimental results indicate that the proposed high-temperature DIC method is easy to implement and can be applied to practical, full-field, high-temperature deformation measurements with high accuracy. © The Authors. Published by SPIE under a Creative Commons Attribution 3.0 Unported License. Distribution or reproduction of this work in whole or in part requires full attribution of the original publication, including its DOI. [DOI: [10.1117/1.OE.53.6.063101](https://doi.org/10.1117/1.OE.53.6.063101)]

Keywords: high-temperature measurement; digital image correlation; sprayed speckle pattern.

Paper 131788 received Nov. 27, 2013; revised manuscript received Mar. 27, 2014; accepted for publication Apr. 2, 2014; published online Jun. 4, 2014.

## 1 Introduction

Carbon fibers represent a large portion of the materials used in aeronautics and aerospace structures, and in the reinforcement of composites. They display a very wide range of thermal, electrical, and mechanical properties: elastic moduli vary between 30 and 900 GPa, and strength can be as high as 6 GPa.<sup>1</sup> Not many research studies have been performed on the properties of the fibers and matrices of carbon at high temperatures.<sup>2,3</sup> In recent years, the thermo-mechanical response of carbon fibers has become an area of great interest among researchers. The high-temperature oxidation behavior of bare and SiC-coated, carbon fiber-reinforced, carbon matrix composites was examined in the temperature range of 900 to 3000 K by Hatta et al.<sup>4</sup> However, the macro performance of the composites was not investigated. A validation study of the thermal expansion and the tensile Young's modulus of carbon steel 1020 at temperatures up to 850°C was measured through using specially designed, high-temperature specimen grips by Codrington et al.<sup>5</sup>

High-temperature deformation measurements are required to characterize the thermo-mechanical response of material systems for thermal protection systems used in aerospace applications. The use of conventional, surface-contacting, strain measurement techniques is not practical in elevated temperature conditions. Technological advancements in digital imaging provide impetus to measure full-field displacement and determine strain fields with subpixel accuracy by image processing.<sup>6</sup> The digital image correlation (DIC) method<sup>7</sup> can provide full-field displacement and surface strain field measurement of an object by comparing two

digital images of the object before and after deformation. The DIC method has been widely used for deformation measurements for many years due to its advantages of only requiring simple equipment, providing very precise results, and ability to obtain noncontact measurements. However, at high temperatures, it is very difficult to prepare the speckle pattern and acquire the images of a distinct speckle pattern. In recent years, many studies have been carried out on high-temperature deformation measurements of the thermo-mechanical response of material systems. Lyons et al. evaluated the ability of the DIC method to measure full-field, in-plane, surface deformations at temperatures up to 600°C.<sup>8</sup> The DIC method was applied for the determination of the coefficient of thermal expansion of films by Bing et al.<sup>9</sup> Grant et al. presented a method that suppressed black-body radiation through the use of filters and blue illumination, which was demonstrated to be capable of providing accurate DIC measurements up to 1100°C.<sup>10</sup> A method that employed a bandpass optical filter to eliminate the influence of black-body radiation of high-temperature objects at 1200°C was published by Bing et al.<sup>11</sup>

In the previous research using the DIC method, the measured temperature was <1200°C because the difficulty of the speckle preparation, and image acquisition increases with increasing temperature. Regarding the original speckle method, the speckle pattern is marked by normal paint and the image is acquired without filters. The normal paint will be volatilized at temperatures of 500°C or greater. Even high-temperature paint will be volatilized at 1200°C. For image acquisition, the aperture used is as small as possible, and no filter is used in the original method. However, because the intensity of the captured image is derived from the black-body radiation of the specimen, the speckle pattern cannot be distinguished by this method. Meanwhile, at high temperatures, i.e., >1200°C, the intensity of the captured

\*Address all correspondence to: Xiang Guo, E-mail: [xianguo1984cn@hotmail.com](mailto:xianguo1984cn@hotmail.com)

image derived from black-body radiation of the specimen is too high to make the image calculable with the DIC method. In this condition, the deformation cannot be calculated by digital image correlation. Therefore, how to produce the stable speckle pattern and acquire a distinct image of speckle pattern is the core problem of DIC the method at high temperatures. In this paper, sprayed tungsten powder is used to prepare the speckle pattern, which is stable at 2600°C. Through the research of the black-body radiation and filters, it was found that filters suppress black-body radiation. Based on the speckle pattern prepared by the sprayed tungsten powder and the images of deformation acquired by using filters, this paper proposes an experimental approach for measuring the thermo-mechanical properties of carbon fibers at temperatures up to 2600°C. The results of the DIC method are compared with the displacement of clamps fixed at both ends of the specimen.

## 2 Experimental Procedure

### 2.1 Speckle Preparation and Image Acquisition

#### 2.1.1 Speckle preparation

Since the surface of the carbon fiber specimen is porous, the original speckle preparation method, which involves painting, is difficult to use, and the process becomes more difficult under high-temperature conditions. Surfaces prepared with the original speckle method cannot stably exist in a high-temperature environment. The inability to produce the stable speckle pattern is the core problem with the DIC method over 1000°C. In this paper, tungsten is used to spray the speckle pattern by a plasma spraying method. Tungsten is an excellent candidate armor material for plasma facing components in nuclear fusion reactors<sup>12</sup> and other equipment operating in high-temperature environments due to its high physical sputtering threshold energy, high melting point (3410°C), low vapor pressure ( $1.3 \times 10^{-7}$  Pa @  $T_{\text{melt}}$ ), good thermal conductivity (180 W/mK),<sup>13-15</sup> and a thermal expansion coefficient that is closer to the thermal expansion coefficient of the carbon material than other materials used in spraying. In this experiment, air was first removed by vacuum, and then the space was filled in with the protective gas to prevent speckle oxidation. The protective gas can steadily maintain the prepared speckle pattern at 2600°C. Figure 1 shows the plasma spraying equipment. The plasma spray approach used in this study has the following advantages:

1. The temperature of the plasma arc is up to 10,000°C. The heat is concentrated, which rapidly melts the materials, such as tungsten, which has a high melting point.
2. The sprayed speckle patterns are stable at 2600°C. In this paper, we use tungsten to spray the speckle pattern. The melting point of tungsten is 3422°C, which is much higher than the temperature of 2600°C at which the experiment was performed.
3. The flow velocity of the plasma flame is up to 1000 m/s, and it will result in spraying powder speeds of up to 180 to 600 m/s; therefore, the bonding strength is very high. The sprayed speckle pattern is difficult to peel off.
4. In the spraying process, the temperature of the specimen is low. The thermal deformation of the specimen can be ignored. The properties of the specimen are not affected.
5. Since carbon and tungsten are two different elements, the emission spectrum is different. Through the filter, the main emission spectrum of tungsten can be filtered out. Thereby, the speckle pattern is formed in the image.

Tungsten particles have a fine spherical structure with a size range of  $\sim 0.5$  to  $1 \mu\text{m}$ .<sup>16</sup> In the spraying process, the tungsten ions will penetrate into the gaps of the carbon fibers and the bonding strength between tungsten and carbon will be very high.

Some studies show that tungsten carbide formation occurs at 1400 to 1600°C; tungsten carbide melts at 2720°C.<sup>17</sup> As reported in other experiments, when the temperature is  $>1400^\circ\text{C}$ , the formation of tungsten carbide begins, and the tungsten carbide is stable at temperatures  $<2720^\circ\text{C}$ . In this paper, the temperature of the experiment is 2600°C, which is lower than the temperature at which tungsten carbide is stable. Consequently, the speckle pattern for the DIC method is stable in this experiment. In this paper, before spraying, a wire mesh is used to cover the surface of the specimen. During the spraying process, the ions pass only through the holes. No tungsten is located on the mesh-covered parts. Since the spraying angle of each part is different, and the size and shape of each mesh is different, the sprayed pattern is formed randomly. The speckle pattern formed by tungsten and carbon fibers is shown in Fig. 2.

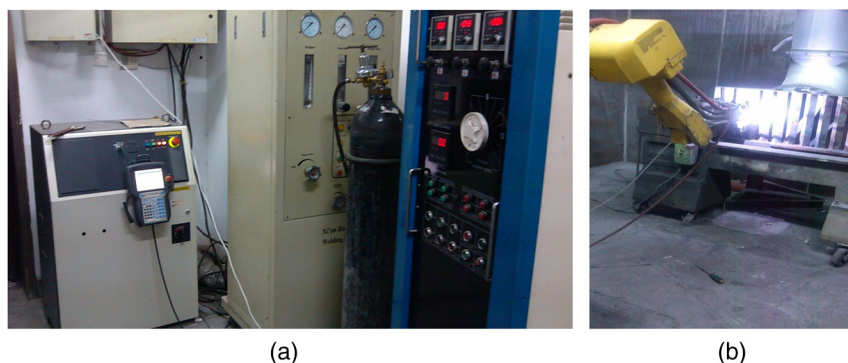
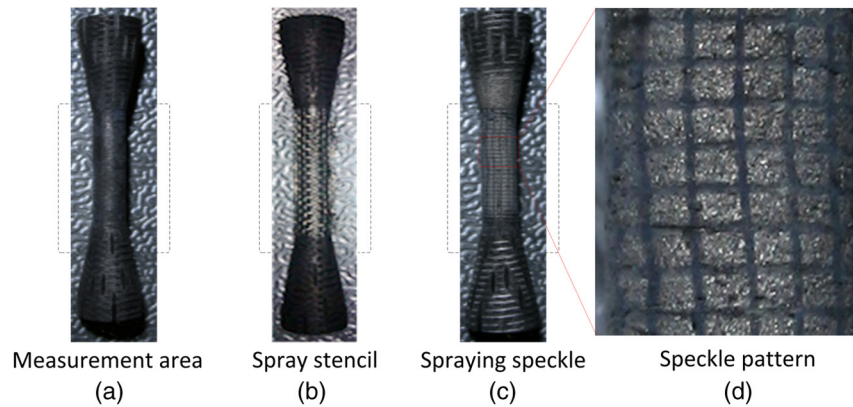


Fig. 1 Spraying. (a) Setting the parameters of spraying. (b) During spraying.



**Fig. 2** Specimen. (a) Measurement area located inside of the dashed rectangle. (b) Stencil of spraying placed on the specimen. (c) Speckle pattern after spraying. (d) Speckle pattern on specimen.

In the spraying process, the temperature of the specimen is low and the thermal deformation of the specimen can be ignored. The properties of the specimen are not affected. Six specimens (three of which are original specimens that were not formed by spraying, and the others are sprayed specimens) are subjected to stretching at room temperature. The rate of extension is 2 mm/min. The tensile test is shown in Fig. 3.

As shown in Fig. 4, the specimen properties are not altered through the hot tungsten during the spraying step. In the first part of the test, at a displacement of  $\sim 0$  to 8 mm, the force is mainly acted on by the core rod. In the second part of the test, at a displacement between 8 and 9 mm, the core rod is broken and the force rapidly decreases. In the third part of the test, at a displacement of  $>9$  mm, the force is mainly acted on by the carbon fiber, as shown in Fig. 5. The curves of speckled and un-speckled specimens are in good agreement.

### 2.1.2 Image acquisition

In theory, in the DIC method, images recorded under different conditions or configurations are analyzed as an optical



**Fig. 3** The tensile test at room temperature of speckled and un-speckled specimens.

metrology. In this sense, the temperatures exerted on the specimen are not a special factor to influence the DIC calculation, provided that good images without any obvious decorrelation effect can be obtained. However, all matter with a temperature greater than absolute zero emits thermal radiation. Thermal radiation (or black-body radiation if the object can be treated as a black body) is electromagnetic radiation generated by the thermal motion of charged particles in matter. When the temperature of the body is greater than absolute zero, interatomic collisions cause the kinetic energy of the atoms or molecules to change. This results in charge acceleration and/or dipole oscillation, which produces electromagnetic radiation, and the wide spectrum of radiation reflects the wide spectrum of energies (ranging from far-infrared to ultraviolet) and accelerations that occur even at a single temperature. As the temperature rises, the thermal radiation emitted by the primary wavelength range, including the shorter and shorter wavelengths range within the sensitive wavelength range of a camera sensor, and the peak wavelength slowly shift to the shorter wavelength side; meanwhile, the total radiation increased very rapidly. For this reason, the brightness of the captured image is intensified.<sup>11</sup> At 2600°C, the intensity of the captured image is mainly derived from black-body radiation of the specimen, and it is too strong to be ignored. Moreover, the intensity of ambient light is far weaker than that of the black-body radiation.

Figure 6 shows the quantum efficiency of the CMOS camera being used in this work, and the camera is sensitive to the wavelength within the 390- to 1050-nm range. In some studies, it can be seen that with temperature increase, several local regions turn bright with apparent intensity changes.<sup>18</sup> When the temperature reaches 2600°C, the light due to thermal radiation intensifies greatly and is far stronger than the ambient light intensity. As a result, the image brightness tends to be saturated and image contrast decreases dramatically, which leads to serious difficulty in recognizing the speckle pattern in the image. This lack of recognition cannot be overcome, even by the most robust DIC algorithm. Consequently, the development of a technique to record high-quality images by suppressing the influence of high-temperature thermal radiation is critical to the deformation measurement at 2600°C temperatures using the DIC method.

In order to clearly elucidate the influence of thermal radiation of a high-temperature object on the intensity of the image captured by an ordinary imaging system, the

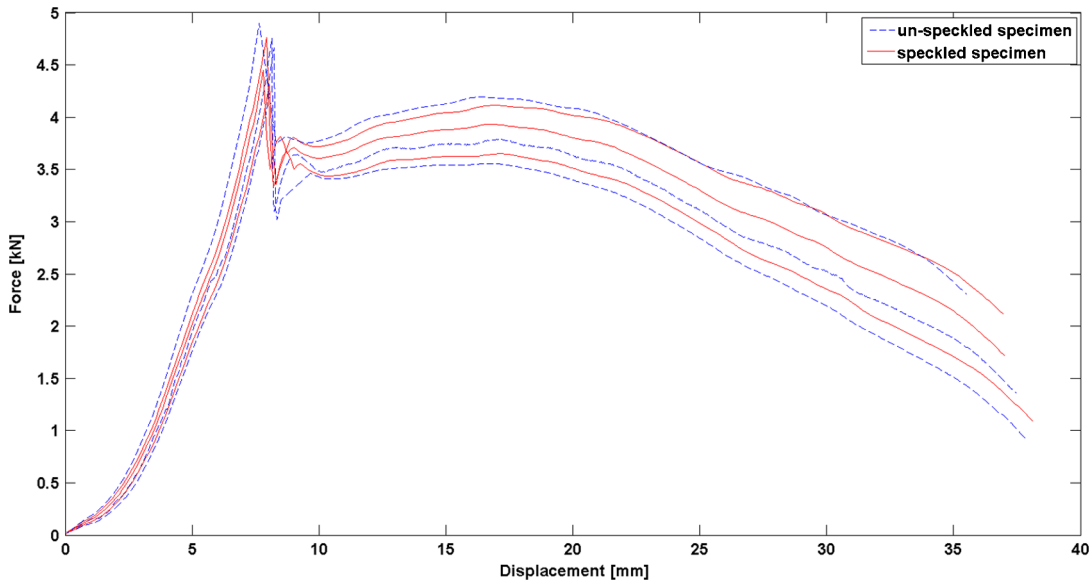


Fig. 4 The comparison of a tensile test at room temperature of speckled and un-speckled specimens.

relationship between thermal radiation energy and temperature is described below. In physics, the spectral energy emitted in the normal direction from a black body at temperature  $T$  at all wavelengths can be quantitatively described using Planck's law in terms of wavelength.<sup>19</sup>

$$I(\lambda, T) = \frac{2hc^2}{\lambda^5} \frac{1}{e^{hc/\lambda kT} - 1}, \quad (1)$$

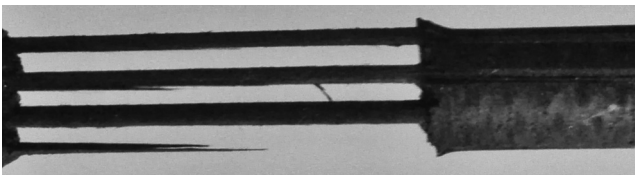


Fig. 5 A broken carbon fiber and core rod.

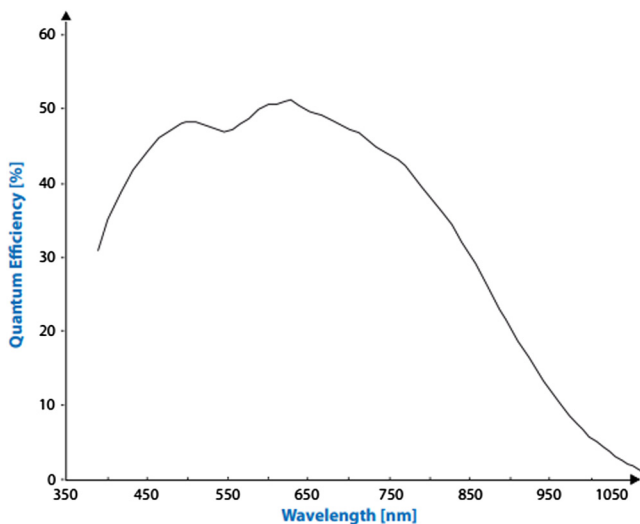


Fig. 6 Quantum efficiency of the CMOS camera used for recording experimental images.

where  $I(\lambda, T)$  is the spectral radiation energy as a function of wavelength  $\lambda$  and temperature  $T$ ,  $h$  is Planck's constant,  $c$  is the speed of light,  $k$  is the Boltzmann constant, and  $e$  is the natural logarithm.

Figure 7 plots the radiation energy as a function of wavelength for temperatures from 1800 to 2600°C according to Planck's law. Note that the radiation energy in Fig. 7 is plotted in logarithmic coordinates. As previously mentioned, Fig. 7 indicates that as the temperature rises, the emitted thermal radiation includes shorter and shorter wavelengths, and the total amount of radiation increases very rapidly. Figure 8 shows the radiation energy as a function of temperature for wavelengths of 450, 550, and 650 nm and it clearly reveals that the radiation energy will increase dramatically as temperature increases.

In spite of the dramatic change in intensity induced by thermal radiation, it is noted that the absolute intensity at short wavelengths (e.g., 450 nm) remains significantly weaker compared with the intensity at relatively longer wavelengths (e.g., 550 and 650 nm). For this reason, when a bandpass

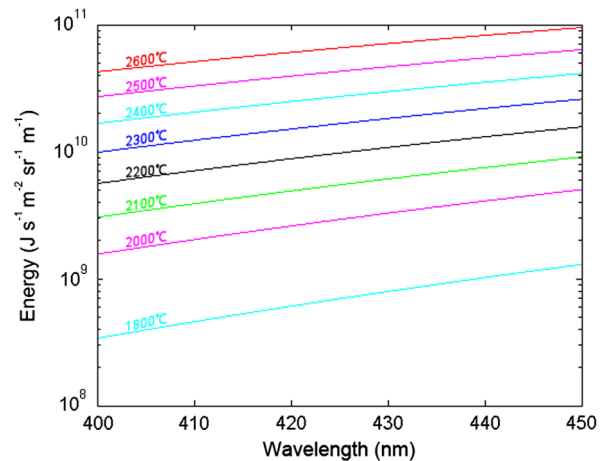
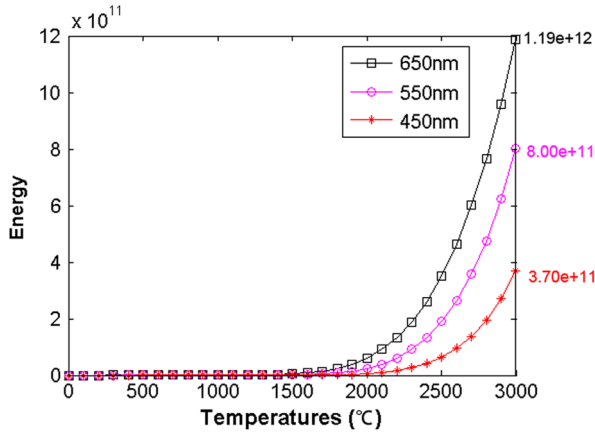


Fig. 7 Thermal radiation energy as a function of wavelength at various temperatures.



**Fig. 8** Thermal radiation energy as a function of temperature for optical wavelength of 450, 550, and 650 nm.

optical filter with a short wavelength is used, it eliminates the light of other wavelengths. Consequently, if a bandpass filter is used, the intensity of the captured image will be significantly reduced. This is a basic idea of the proposed approach for handling the thermal radiation issue.

Due to the different elements of carbon and tungsten, there is a certain difference between the spectra of the radiation emitted at high temperatures. Meanwhile, since carbon was used as the main body of the specimen and tungsten only existed on the surface, the intensity of the radiation of tungsten at high temperatures was far below the intensity of carbon. Accordingly, by the suppression of the intensity of the radiation, tungsten radiation will be reduced to form the black portion of the speckle pattern, and the carbon will form the white portion, i.e., the distinct speckle formed on the specimen surface.

As Figs. 9 and 10 show, along with the rise in temperature, in the radiation spectrum of the pure carbon specimen, the light intensity at 600 nm was significantly increased; the radiation spectrum of the specimens sprayed with tungsten has a second peak at 695 nm. At 2600°C, compared with the radiation spectra of carbon fiber specimens not sprayed with tungsten and carbon fiber specimens sprayed with

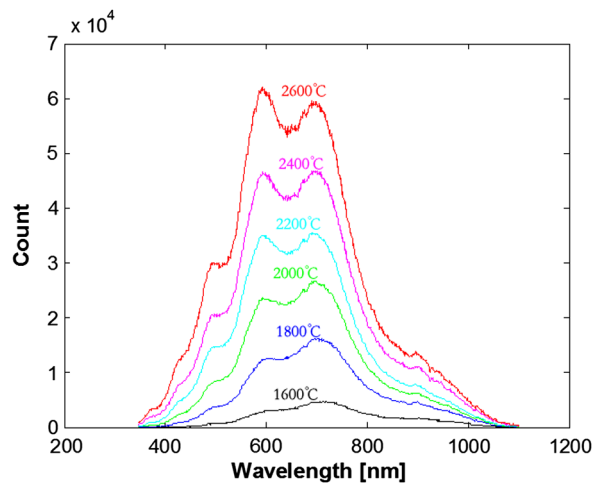


**Fig. 9** Spectra of carbon fiber specimens not sprayed with tungsten at different temperatures.

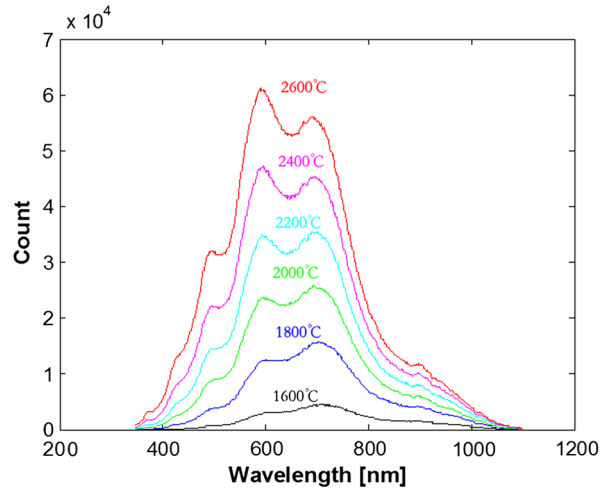


**Fig. 10** Spectra of carbon fiber specimens sprayed with tungsten at different temperatures.

tungsten, the intensity is slightly enhanced at the 695-nm wavelength. Due to the small difference in the intensity of light at the 450-nm wavelength, the radiation energy of tungsten can be ignored at the 450-nm wavelength, and the black spots of the speckle pattern will be formed by tungsten by suppressing the intensity of black-body radiation. In this paper, the wavelength of a 450-nm bandpass filter (the transmission spectrum is shown in Fig. 11 and Table 1), neutral filters, and polarizing filters are used to suppress the intensity of black-body radiation; thereby, the speckle texture is formed by black spots of sprayed tungsten and white spots of carbon.

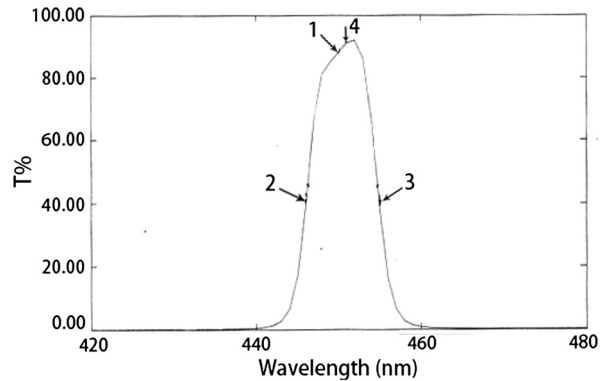


**Fig. 11** The transmission spectrum of the 450-nm bandpass filter.

**Table 1** The transmission spectrum of the 450-nm bandpass filter.

No.	Wavelength (nm)	Transmittance (%)
1	450.00	87.930
2	446.00	39.462
3	455.00	29.918
4	451.00	91.203

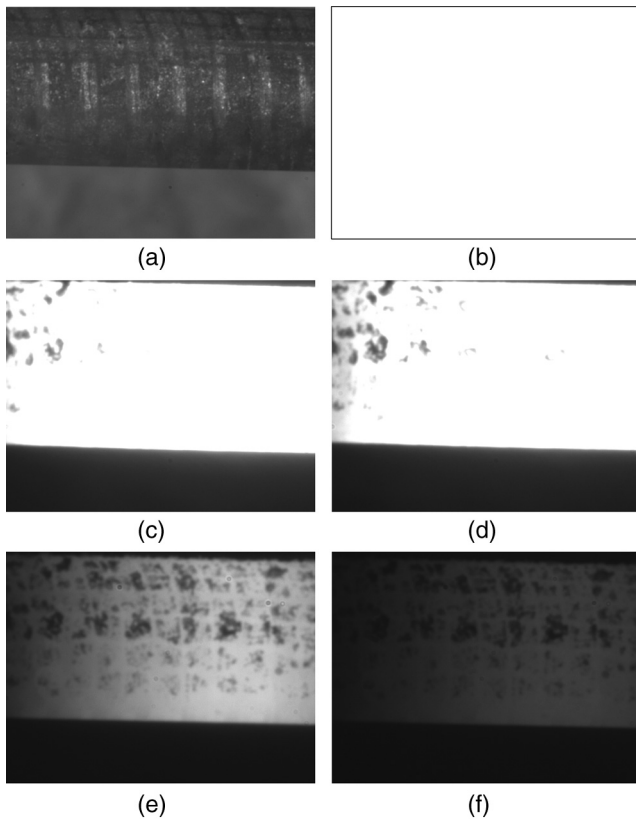


**Fig. 12** Image of a specimen (a) acquired at room temperature; (b) acquired without filter at 2600°C; (c) acquired with one linear polarizing (PL) filter at 2600°C; (d) acquired with one 450-nm bandpass and one PL filter at 2600°C; (e) acquired with two ND8 filters, one 450-nm bandpass filter, and one PL filter at 2600°C; (f) acquired with two ND8 filters, one PL filter, one ND2 filter, one ND4 filter, and one 450-nm bandpass filter at 2600°C.

In image acquisition, although reducing the exposure time of the camera and aperture of the lens can reduce the intensity of the image, it is difficult to distinguish between carbon and tungsten. Some studies used bandpass filters in acquisition near 1100°C.<sup>11</sup> However, at 2600°C, the light of carbon radiation suppressed by the bandpass filter is still too high and the tungsten is difficult to distinguish from the captured image by the diffused light. In this paper, a linear polarizing filter and a neutral density (ND) filter are used to suppress black-body radiation in conjunction with the bandpass filter. In the acquisition process, the ND filters and linear polarizing (PL) filter are also very critical components in image acquisition at high temperatures. As Fig. 12(d) shows, the bandpass filter can reduce the intensity of the captured image, but the reduction is still not enough for the DIC method. Because of the principle limitation of the bandpass filter, the superposition of the bandpass filter cannot produce a more significant reduction than a single filter for the intensity of the captured image. Therefore, it is necessary to use other types of filters to achieve suppression of black-body radiation.

As Fig. 13 and Table 2 show, for an ND filter with optical density  $d$ , the amount of optical power transmitted through the filter, which can be calculated from the logarithm of the ratio of the measurable intensity ( $I$ ) after the filter to the incident intensity ( $I_0$ ),<sup>20</sup> is calculated as follows:

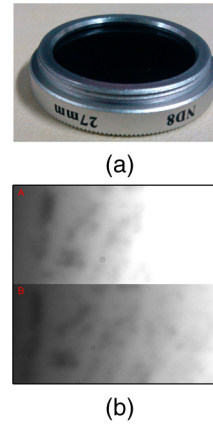


**Fig. 13** Neutral density filter. (a) Neutral density filter. (b) Comparison image of neutral density filters: B is acquired with one ND8 increased.

**Table 2** The transmittance of neutral density filters.

	Lens area opening, as fraction of the complete lens	Optical density	f-stop reduction	Percent transmittance (%)
	1	0.0		100
ND2	1/2	0.3	1	50
ND4	1/4	0.6	2	25
ND8	1/8	0.9	3	12.5

$$d = -\log_{10}(I/I_0). \tag{2}$$

For each ND filter, the intensity of light is significantly reduced. The advantage of the ND filter is that the effect of the neutral density can be superposed in order to further reduce the light intensity. However, there is a problem with the ND filters in that the neutral density filters reduce the intensity of all wavelengths equally. If the bandpass filter is not used, the speckle pattern in the captured image will not be identified clearly. Likewise, if there are no ND filters in the acquisition, the speckle pattern in the captured image will be completely covered by white halos. Therefore, in the acquisition system at high temperatures, the bandpass filter and ND filters are equally important and indispensable.

ND8 can reduce the light intensity linearly. For this figure, the intensity of the image B is only 12.5% of the unused ND8 (image A). The left side of image B is darker than the left side of image A. The right side of image B is clearer than the right side of image A. It shows that the ND filter is necessary in the acquisition system at high temperatures.

When the specimen was heated in a high-temperature test chamber, the black-body radiation continuously reflected on the walls of the chamber. In the captured image, the information on the speckle pattern is overwhelmed by the clutter of reflected light. The speckle texture cannot be clearly identified due to the interference effect of the light. A polarizer is an optical filter that passes light of a specific polarization and blocks waves of other polarizations.<sup>21</sup> As Fig. 14 shows,

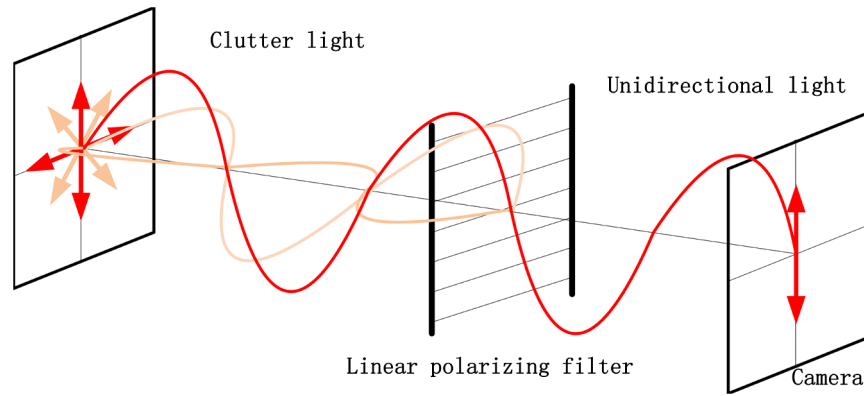


Fig. 14 Linear polarizing filter.

a wire-grid polarizer converts an unpolarized beam into one with a single linear polarization. Colored arrows depict the electric field vector. The diagonally polarized waves also contribute to the transmitted polarization. Their vertical components are transmitted, while the horizontal components are absorbed and reflected.

As Fig. 14 shows, Malus’s law, which is named after Étienne-Louis Malus, says that when a perfect polarizer is placed in a polarized beam of light, the intensity,  $I$ , of the light that passes through is given by

$$I = I_0 \cos^2 \theta_i, \tag{3}$$

where  $I_0$  is the initial intensity and  $\theta_i$  is the angle between the initial polarization direction of the light and the axis of the polarizer. In Figs. 14 and 15,  $\theta_i = \theta_1 - \theta_0$ .

Using polarizing filters reduced the intensity of the captured image and the interference effects of the light. In the high-temperature experiments, a couple of polarizing filters were used; one was installed on the observation window and another was installed on the lens. The polarization of light through the chamber will be captured.

As shown in Fig. 12, PL stands for linear polarizing filter; and D2, ND4, and ND8 are three different ND filters. Before acquisition, even if the exposure time of the camera and aperture of the lens are set as low as possible, the intensity is still too high to distinguish between the carbon and tungsten. The reason for this phenomenon is that the intensity of radiation of carbon is too high and the light is not parallel. For this reason, the tungsten is overwhelmed by the light of radiation from the carbon. Figure 12(a) is acquired at room temperature. In this image, the black spots are carbon fibers and the white spots are tungsten powder. The other images are acquired with different filter conditions at 2600°C. In these images, the black spots are tungsten powder, and the white spots are carbon fibers. According to Figs. 12(a)

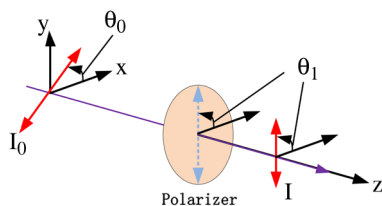


Fig. 15 Polarization of light.

and 12(b), as a result of using an ordinary imaging system, the similarity between the reference image recorded at room temperature and any image recorded at a temperature >2600°C decreases dramatically, making the DIC analysis fail to obtain reliable results. According to Figs. 12(c), 12(d), 12(e), and 12(f), a single filter cannot effectively reduce the light intensity, so a series of filters is a necessary component of an acquisition system. When the temperature is <2600°C, the ND filters should be changed for image acquisition. As Figs. 16 and 17 show, it is proven that after the bandpass filter is applied, the brightness of the captured image is mainly formed by the carbon. Meanwhile, if the PL and neutral filters are not used in the acquisition process, the intensity of the captured image is still too high based on the diffused light coming from the radiation of the carbon.

### 2.2 Digital Image Correlation Method

In image correlation,<sup>22</sup> the matched position of the random speckle pattern is obtained in different deformation stages by optimal correlation.<sup>23,24</sup> As shown in Fig. 18, in the reference image, it is selected such that a square reference subset of  $(2M + 1) * (2M + 1)$  pixels is centered at point  $P$ . In the other deformed images, the procedure of matching is to find the corresponding subset centers as point  $P'$ . The corresponding subset in the deformed image should

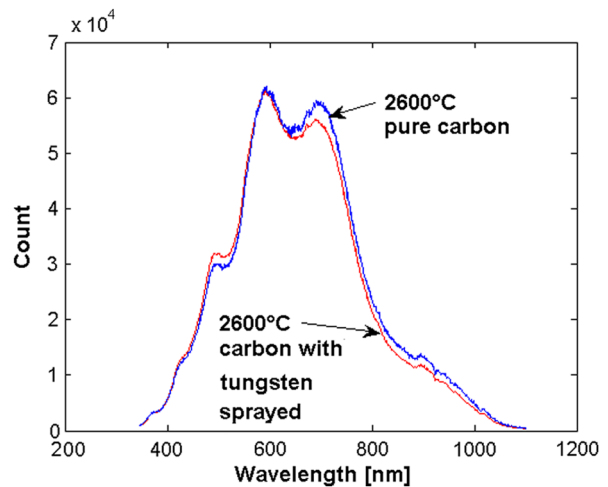


Fig. 16 Spectra of carbon fiber specimens not sprayed with tungsten and carbon fiber specimens sprayed with tungsten at 2600°C.

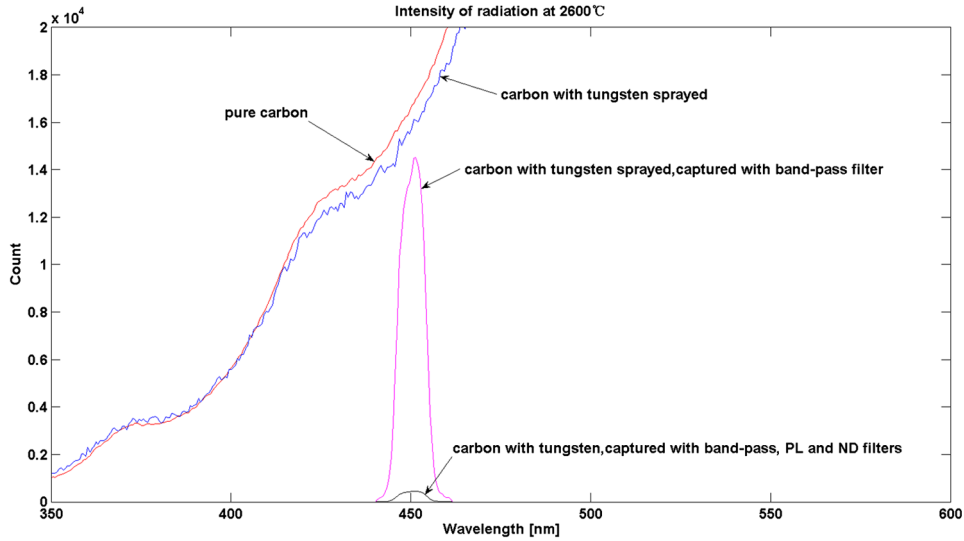


Fig. 17 Intensity of radiation at 2600°C.

have the maximum amount of similarity with the reference subset. Consequently, the two center points of the deformed and reference subsets ( $P$  and  $P'$ ) are a couple of corresponding points in two images. A predefined cross-correlation (CC) criterion or sum of squared differences (SSD) criterion<sup>25</sup> is used to evaluate the similarity between the reference subset and the target subset. So, the corresponding subset location can be determined by searching the maximum or minimum (according to the used CC) CC in the specified searching area.

Due to its simplicity, the SSD correlation is adopted in this work.

$$C_{SSD}(p) = \sum_{x=-M}^{x=M} \sum_{y=-M}^{y=M} [f(x, y) - r_0 - r_1 * g(x', y')], \quad (4)$$

where  $f(x, y)$  is the gray value of point  $(x, y)$  in the reference subset of the reference image,  $g(x', y')$  is the gray value of point  $(x', y')$  in the corresponding subset of the deformed image,  $r_0$  and  $r_1$  are used to compensate the gray value difference caused by illumination diversity, and  $p = [u, u_x, u_y, v, v_x, v_y, r_0, r_1]$  represents the vector of the correlation parameters that depends on the chosen mapping function. The first-order mapping function is used in this work.

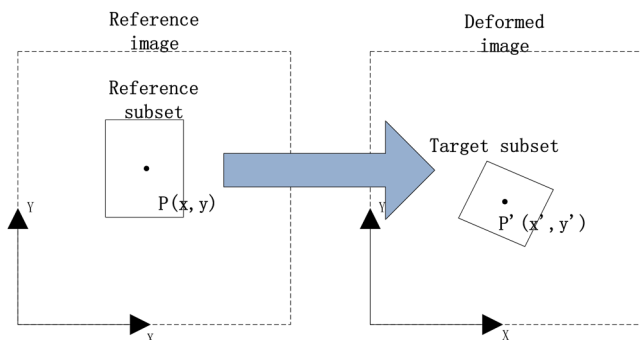


Fig. 18 The basic principle of digital image correlation.

$$\begin{aligned} x'_i &= x_0 + \Delta x + u + u_x \Delta x + u_y \Delta y \\ y'_i &= y_0 + \Delta y + v + v_x \Delta x + v_y \Delta y, \end{aligned} \quad (5)$$

where  $\Delta x$  and  $\Delta y$  are the distances from the subset center to point  $(x_i, y_i)$ ,  $u$  and  $v$  are the displacement components of the reference subset center in the  $x$  and  $y$  directions, and  $u_x$ ,  $u_y$ ,  $v_x$ , and  $v_y$  are the first-order displacement gradients of the reference subset.

Obtaining the minimum  $C_{SSD}$  is a nonlinear minimization problem, which can be solved by using the iterated local search (ILS) algorithm.<sup>26</sup> Still, it needs to be pointed out that a bicubic spline interpolation<sup>27</sup> is adopted in the algorithm realization because the coordinates of points in the deformed image are not integer pixels. Moreover, to evaluate the accuracy of the ILS results, the standard deviation can be employed.

$$s_0 = \sqrt{\frac{\sum \sum v^2}{n-1}}, \quad (6)$$

where  $n$  is the number of pixels in the reference subset, and  $v$  represents the gray value residual of one pixel after the correlation calculation. In this paper, an optimized correlation routine was used by employing the Newton-Raphson method with differential corrections to minimize search time.

### 2.3 Strain Calculation

The calculation of strain is relatively complex. As shown in Fig. 19, the coordinates of eight neighboring points are used to calculate the strain of point  $P$ . The details of the calculation steps are as follows:

1. In the reference stage, the point  $P$  and the neighboring points are used to obtain a set of two-dimensional (2-D) points ( $P_r$ ) in a 2-D coordinate system  $OXY$ .
2. Exactly the same process in the current stage is repeated, and a set of 2-D points ( $P_c$ ) in a 2-D coordinate system  $O'X'Y'$  is obtained.

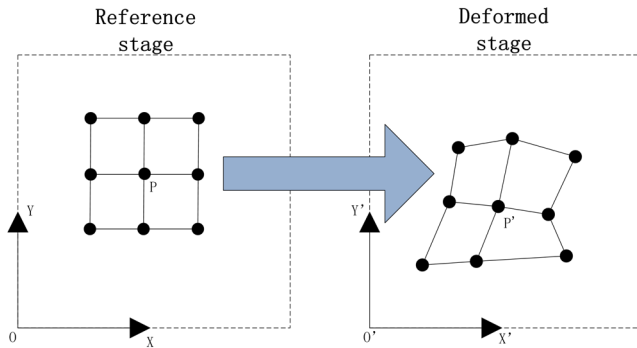


Fig. 19 Strain calculated using points.

3. The deformation gradient tensor  $F$  ( $2 \times 2$  matrix) is calculated using the two sets,  $P_r$  and  $P_c$ . They have a functional relationship as follows:

$$P_c = u + F \bullet P_r, \quad (7)$$

where  $u$  stands for the rigid body translation between  $P_r$  and  $P_c$ . To solve for  $F$ , a standard least-squares algorithm can be adopted. The deformation gradient tensor  $F = RU$  can be split to the rotation matrix  $R$  and stretch tensor  $U$ , and the strain of point  $P$  in the current stage can be acquired from  $U$  directly in

$$U = \begin{pmatrix} 1 + \epsilon_x & \epsilon_{xy} \\ \epsilon_{xy} & 1 + \epsilon_y \end{pmatrix}. \quad (8)$$

Due to temperature fluctuations during the experiment, it is necessary to consider the impact of thermal expansion. In thermal strain measurement of homogeneously expanded materials, the average of strains at all calculated points can be taken as the thermal strain.<sup>28-30</sup> In this paper, however, in order to better alleviate the influence of noise and eliminate in-plane rigid-body rotation, a linear surface fitting algorithm is employed to approximate the entire computed displacement field. Consequently,  $M$  in Eq. (5) denotes a set containing all valid data points in the field. In this way, the determined small rotation angle ( $\omega$ ) can be used to eliminate the inevitable in-plane rigid-body rotation occurring during free thermal expansion of the specimen to show the pure thermal expansion.

After obtaining the discrete thermal strains associated with various temperatures, the actual strain of the specimen can be calculated as

$$\epsilon_{\text{actual}} = \epsilon_{\text{DIC}} - \epsilon(T). \quad (9)$$

### 3 Experiment Results

In this experiment, the specimen was heated to 2600°C by electric current at first, and then the specimen was stretched until fracturing in a 2600°C environment. As Fig. 20 shows, during the deformation process, a CMOS camera was used to acquire images of the deformation process. The camera was placed outside the chamber and the filters were fixed on the lens. The DIC method was used to calculate the strain field of the specimen during deformation. In the deformation process, the displacement of the stretching clamp is recorded

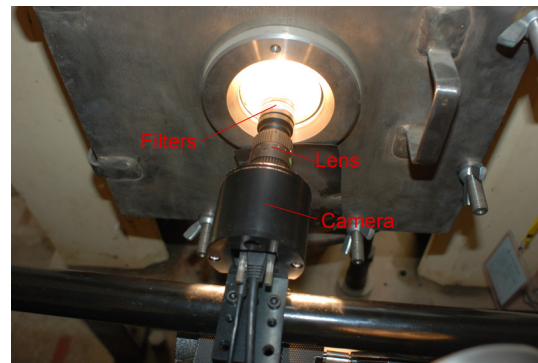


Fig. 20 Acquisition system.

as extensometers and compared with the calculated result of the digital image correlation method.

Because the heating and deformation of the specimen occurs in the chamber, a telephoto lens (75 mm focal length) is used with the filters. Images are acquired through the observation window on the chamber. As Fig. 20 shows, the specimen is illuminated at high temperatures and the external light source is redundant during the experiment. In the experiment, the camera, lens, and filters are outside the cabinet. The outside temperature is below the permissible temperature of the lens and camera. Accuracy has no significant effect.

In this paper, the thermoscope is used to measure the temperature of the center position of specimen. The closed-loop control is formed by adjusting the current value to ensure that the temperature is stable at 3200°C. The temperature controlled cabinet and the thermoscope are shown in Fig. 21. The heating and stretching devices is shown in Fig. 22. The Schematic diagram of experiment is shown in Fig. 23. The dimension of specimen is shown in Fig. 24. The clamping method of specimen is shown in Fig. 25.

In the experiment, the air of the high-temperature chamber is pumped out by vacuum first, and then the area is filled with protective gas to prevent the reaction of tungsten at high temperatures.

As shown in Fig. 26, it can clearly be seen that the sprayed target is still stably preserved after being heated to 2600°C. For comparison, when the heating temperature is raised to 3200°C, only a few targets remain. The reason for this is that tungsten carbide is produced in the heating process

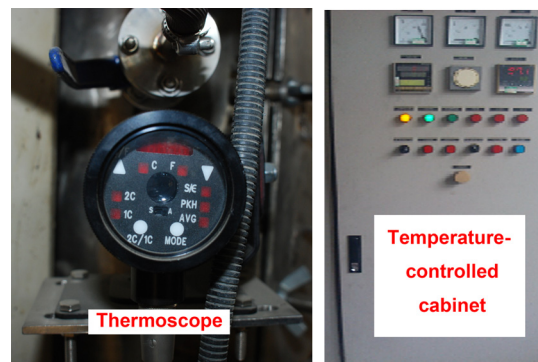


Fig. 21 Temperature measurement and control components for the closed-loop control of temperature.



Fig. 22 Heating and stretching devices.

and is melted when the temperature is higher than its melting point. However, 2600°C is lower than the melting point of tungsten carbide. So, the sprayed target can be stably preserved at 2600°C.

In order to verify the accuracy of DIC, the clamps are used as an equivalent extensometer. Before the experiment starts, the distance between clamps is measured as the initial position  $l_0$ . During the experiment, the displacement of the upper clamp is recorded as  $l_i$ . The deformation of the distance between clamps is calculated as the extensometer and compared with the speckle measurement result. The deformation between clamps can be calculated as

$$e_i = (l_i - l_0)/l_0. \quad (10)$$

For comparison with the equivalent extensometer, the strain data used to compare are the averaged value of measurement field. Prior to the experiment, the camera was

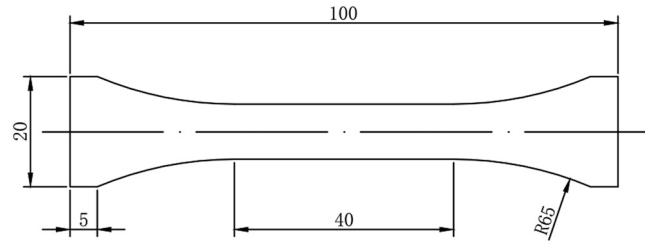


Fig. 24 Specimen.

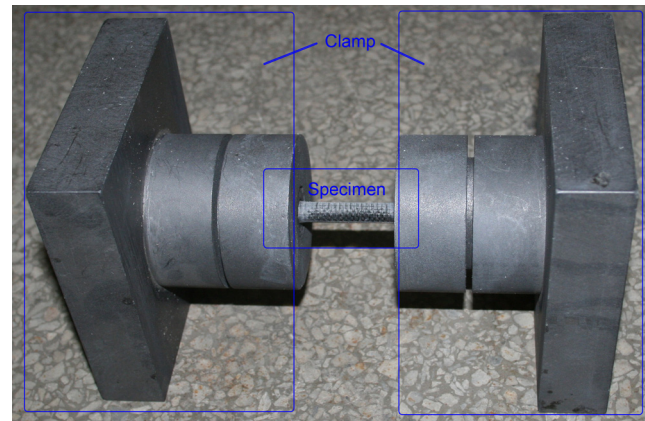


Fig. 25 Specimen before heating.

aligned to the center position of the specimen. For the rod specimen, it is only required that the optical axis of the camera is perpendicular to the axis of the specimen. As Fig. 27 shows, before the experiment starts, there is small deformation of the specimen with the clamping device chuck. There are two stages of the whole deformation process: the elastic deformation stage and the plastic deformation stage. In the elastic deformation stage, the deformation of the overall specimen is substantially uniform. The measured strain of

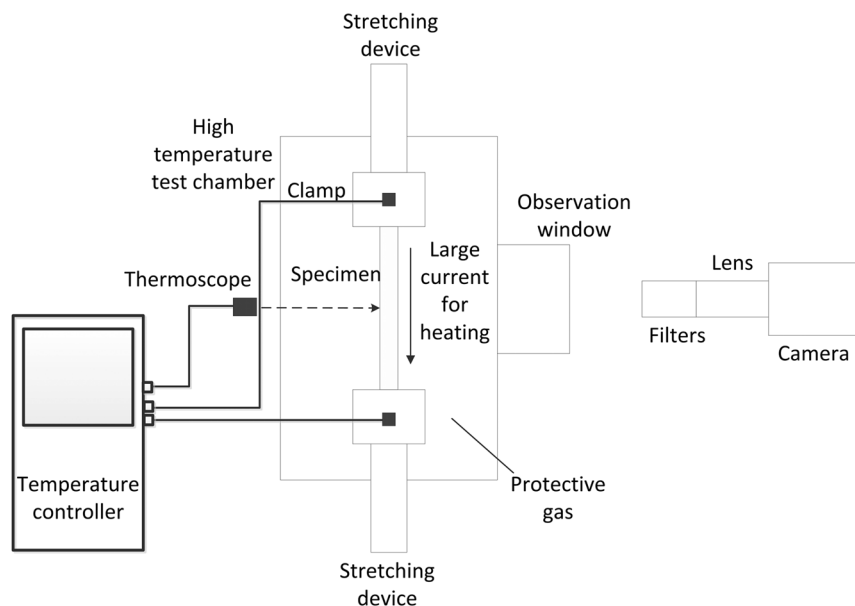


Fig. 23 Schematic diagram of experiment.

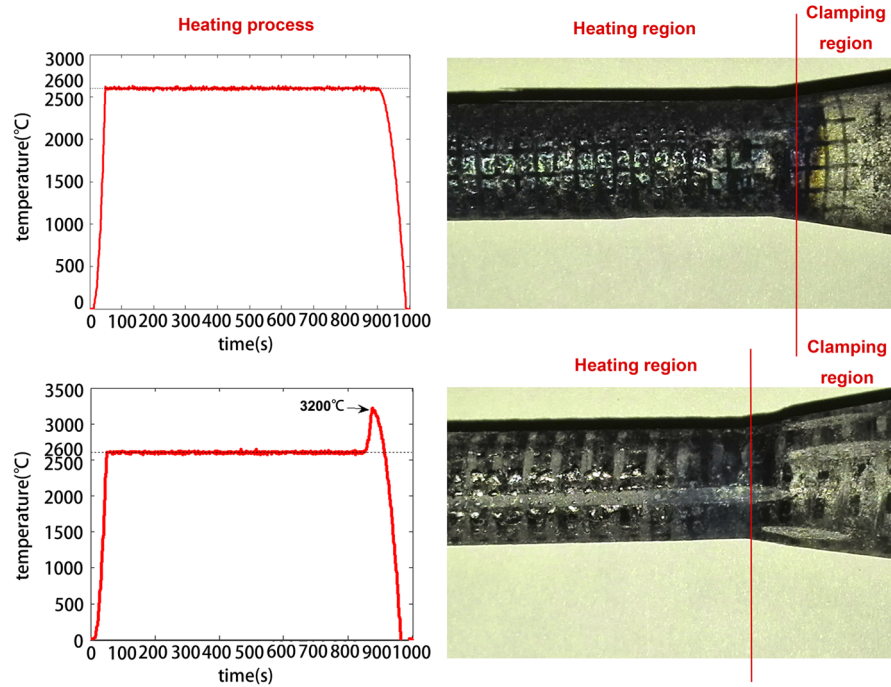


Fig. 26 Specimen after heating.

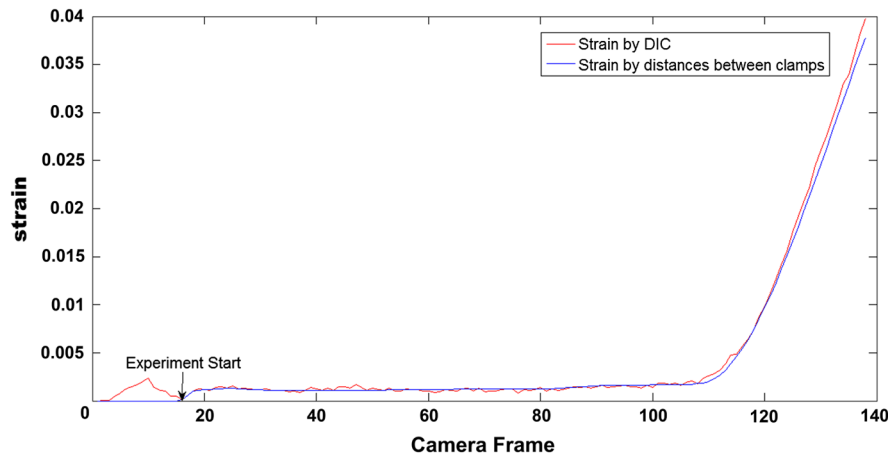


Fig. 27 Digital image correlation result compared with displacement of clamps.

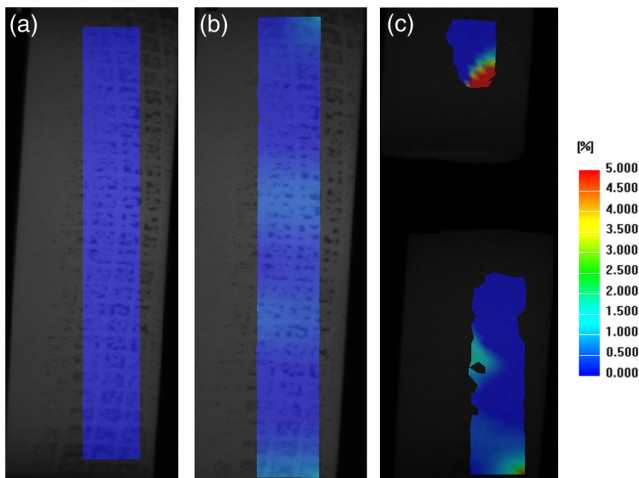


Fig. 28 Strain field of the specimen during stretching.

the speckles is substantially equivalent to the strain calculated according to the equivalent extensometer. In the plastic deformation stage, due to the uneven distribution of the deformation field, the strain is calculated according to the equivalent extensometer, which is less than the strain calculated with the speckle pattern. In the plastic deformation stage, the closer the fracture location, the more the strain. The field of the DIC measurement is smaller and closer to the fracture location than the field between the clamps, so the DIC result in the plastic deformation stage is higher than the result of the equivalent extensometer. According to the comparison between the two curves, the result of the DIC measurement is correct and plausible.

Figure 28(a) shows the instant at which the experiment starts, where the strain at this point in time is 0. Figure 28(b) shows the stage at which the average strain is 0.16% and uneven deformation of the specimen occurs. Figure 28(c) shows the time at which the specimen broke.

After fracture, the temperature falls sharply, and the image turns dark. It can be seen that the deformation is the greatest at the lower section of the upper part, and the overall deformation there is 3.81%.

#### 4 Conclusion

A simple, easy-to-implement, yet effective high-temperature DIC technique was evaluated for noncontact and full-field deformation measurement of high-temperature objects in this study. By virtue of the plasma spray for speckle preparation and the filters for image acquisition, high-quality digital images of the object at temperatures up to 2600°C can be readily acquired, and these images can be directly processed by the well-established DIC algorithm to extract full-field deformation with high fidelity. The deformation of stretching at 2600°C is measured and compared with the displacement between clamps, confirming the effectiveness and accuracy of the proposed technique. The results of this work indicate that the proposed high-temperature DIC technique is capable of accurately measuring full-field deformation at temperatures up to 2600°C. At temperatures ranging from stimulated emission temperature to at least 2600°C, the method can be used with different ND filters. Experimental results indicate that the proposed high-temperature DIC method is easy to implement and can be applied to practical, full-field, high-temperature deformation measurements with high accuracy. It is also worth noting that the studied high-temperature DIC method can be combined with other thermal loading devices to obtain deformation measurement at higher temperatures.

#### Acknowledgments

The authors acknowledge the support of the National Natural Science Foundation of China (Grant No. 51275378 and 51275389) and the Science and Technology Innovation Project of Jiangsu Province (SBC201210069).

#### References

- C. Sauder, J. Lamon, and R. Pailler, "Thermomechanical properties of carbon fibres at high temperatures (up to 2000 °C)," *Compos. Sci. Technol.* **62**(4), 499–504 (2002).
- Y. Tanabe et al., "The strength of pitch-based carbon fibre at high temperature," *J. Mater. Sci.* **26**(6), 1601–1604 (1991).
- M. Trinquecoste et al., "High temperature thermal and mechanical properties of high tensile carbon single filaments," *Carbon* **34**(7), 923–929 (1996).
- H. Hatta et al., "High-temperature oxidation behavior of SiC-coated carbon fiber-reinforced carbon matrix composites," *Compos. Part A Appl. Sci. Manuf.* **30**(4), 515–520 (1999).
- J. Codrington et al., "Induction heating apparatus for high temperature testing of thermo-mechanical properties," *Appl. Thermal Eng.* **29**(14–15), 2783–2789 (2009).
- J. E. Cline, "Development of ultra-high temperature material characterization capabilities using digital image correlation analysis," University of Texas at Arlington, MS (2011).
- T. Chu, W. Ranson, and M. Sutton, "Applications of digital-image-correlation techniques to experimental mechanics," *Exp. Mech.* **25**(3), 232–244 (1985).
- J. S. Lyons, J. Liu, and M. A. Sutton, "High-temperature deformation measurements using digital-image correlation," *Exp. Mech.* **36**(1), 64–70 (1996).
- P. Bing et al., "Measurement of coefficient of thermal expansion of films using digital image correlation method," *Polym. Test.* **28**(1), 75–83 (2009).
- B. M. B. Grant et al., "High-temperature strain field measurement using digital image correlation," *J. Strain Anal. Eng. Des.* **44**(4), 263–271 (2009).
- P. Bing et al., "High-temperature digital image correlation method for full-field deformation measurement at 1200 °C," *Meas. Sci. Technol.* **22**(1), 015701 (2011).
- H. Jianjun et al., "Properties of tungsten coating deposited onto copper by high-speed atmospheric plasma spraying," *J. Nucl. Mater.* **414**(1), 8–11 (2011).
- K. Tokunaga et al., "Behavior of actively cooled mock-ups with plasma sprayed tungsten coating under high heat flux conditions," *Fusion Eng. Des.* **81** A(1–4), 133–138 (2006).
- N. Yoshida, "Review of recent works in development and evaluation of high-Z plasma facing materials," *J. Nucl. Mater.* **266–269**, 197–206 (1999).
- I. Smid et al., "Development of tungsten armor and bonding to copper for plasma-interactive components," *J. Nucl. Mater.* **258–263**(Part 1), 160–172 (1998).
- A. Abu-Oqail et al., "Effects of processing parameters of tungsten-copper composites," *Int. J. Refract. Metals Hard Mater.* **35**, 207–212 (2012).
- Z. F. Queiroz et al., "Surface and gas phase temperatures of a tungsten coil atomizer," *Spectrochim. Acta Part B At. Spectrosc.* **57**(11), 1789–1799 (2002).
- B. Pan, D. Wu, and Y. Xia, "High-temperature deformation field measurement by combining transient aerodynamic heating simulation system and reliability-guided digital image correlation," *Opt. Lasers Eng.* **48**(9), 841–848 (2010).
- G. B. Rybicki and A. P. Lightman, *Radiative Processes in Astrophysics*, Wiley-VCH, New York (1979).
- R. Hanke, *Filter-Faszination (Filter-Faszination, engl.) All about filter and their use in still, movie and television photography*, Hama, Monheim, Bayern, Germany (1979).
- V. Torres-Zúñiga et al., "Optical absorption photoacoustic measurements for determination of molecular symmetries in a dichroic organic-film," *Opt. Express* **16**(25), 20724–20733 (2008).
- B. Pan, Z. Lu, and H. Xie, "Mean intensity gradient: an effective global parameter for quality assessment of the speckle patterns used in digital image correlation," *Opt. Lasers Eng.* **48**(4), 469–477 (2010).
- M. A. Sutton, J.-J. Orteu, and H. W. Schreier, *Image Correlation for Shape, Motion and Deformation Measurements: Basic Concepts, Theory and Applications*, Springer, USA (2009).
- Z. Tang et al., "Large deformation measurement scheme for 3D digital image correlation method," *Opt. Lasers Eng.* **50**(2), 122–130 (2012).
- B. Pan, H. Xie, and Z. Wang, "Equivalence of digital image correlation criteria for pattern matching," *Appl. Opt.* **49**(28), 5501–5509 (2010).
- B. Pan et al., "Digital image correlation using iterative least squares and pointwise least squares for displacement field and strain field measurements," *Opt. Lasers Eng.* **47**(7–8), 865–874 (2009).
- M. Sutton et al., "Advances in two-dimensional and three-dimensional computer vision," in *Photomechanics*, P. Rastogi, Ed., pp. 323–372, Springer, Berlin, Heidelberg (2000).
- N. Li et al., "Full-field thermal deformation measurements in a scanning electron microscope by 2D digital image correlation," *Exp. Mech.* **48**(5), 635–646 (2008).
- T. A. Berfield et al., "Thermal strain measurement in sol-gel lead zirconate titanate thin films," *J. Appl. Phys.* **106**(12), 123501–123507 (2009).
- M. De Strycker et al., "Measuring the thermal expansion coefficient of tubular steel specimens with digital image correlation techniques," *Opt. Lasers Eng.* **48**(10), 978–986 (2010).

**Xiang Guo** is a doctoral student of Xi'an Jiaotong University. His research field is in optical measurement.

**Jin Liang** is a professor of Xi'an Jiaotong University. His research field is in optical measurement.

**Zhengzong Tang** is a doctor of Xi'an Jiaotong University. His research field is in optical measurement.

**Binggang Cao** is a professor of Xi'an Jiaotong University. His research field is in electric vehicle control technology and electro-mechanical control systems.

**Miao Yu** is a master's student of Xi'an Jiaotong University. His research field is in optical measurement.